Proceedings of International Conference on Heat Exchanger Fouling and Cleaning - 2015 (Peer-reviewed)
June 07 - 12, 2015, Enfield (Dublin), Ireland
Editors: M.R. Malayeri, H. Müller-Steinhagen and A.P. Watkinson

Published online
www.heatexchanger-fouling.com

PLATE-FIN HEAT EXCHANGER FOULING IDENTIFICATION USING D-OPTIMAL EXPERIMENTAL DESIGN

K. A. Palmer, W. T. Hale, and G. M. Bollas[*]
[*]Department of Chemical & Biomolecular Engineering, University of Connecticut, Storrs, 191 Auditorium Road, Unit 3222, Storrs, CT, 06269-3222, USA, george.bollas@uconn.edu

ABSTRACT

Fouling is a notable problem for aircraft heat exchangers in high-debris environments. Monitoring heat exchanger fouling levels is essential for aircraft maintenance scheduling and safety. In this document, methods for offline fouling identification during aircraft ground handling are explored to utilize a broader range of inputs than what is available during flight. Optimal experimental design is applied to a cross-flow plate-fin heat exchanger model of an environmental cooling system to find input trajectories that can maximize fouling identification capabilities. A model is developed for this analysis that accounts for mass, momentum and energy balances, validated with reported data and then applied to a dynamic sensitivity analysis framework. The sensitivities of the measured outputs with respect to fouling-related uncertainties are maximized by adjusting controllable inputs within specified design constraints. This method is assessed by a comparison of the confidence intervals of the estimated thermal fouling resistance through a series of case studies that examine uncertain environmental conditions.

INTRODUCTION

An environmental control system (ECS) serves the essential purpose of providing fresh air at appropriate conditions (determined by factors such as current altitude, aircraft flight path, etc.) to the passengers and crew. It is also responsible for additional tasks such as component heating and cooling, anti-icing, de-misting and rain dispersion. ECSs control the hot, compressed “bleed” air stream coming from the aircraft engines in traditional designs or from a “ram” air stream compressor in more modern designs (Moir & Seabridge, 2008).

The majority of aircraft ECSs control the hot air stream with cross-flow plate fin heat exchangers due to their excellent heat transfer efficiency in relation to their small weight and volume (Kays & London, 1984). Using ambient ram air as the cold side fluid, these air-cooled heat exchangers of an ECS decrease the temperature of the hot stream. However, as a result of using ambient air as the cold side fluid, the ECS, and in particular the cold side of the heat exchanger, is exposed to fouling contaminants like sand, dust and salt (Moir & Seabridge, 2008; Wright et al., 2009).

Aircraft ECS fouling typically occurs through particle deposition onto components when the aforementioned contaminants are present in the inlet airflow streams. The accumulation of these particles are functions of the inlet stream airflow rate, temperature, pressure and the contaminant concentration (Shah & Sekuli, 2003). Particle deposition onto the ECS heat exchanger surface over time results in the reduction of heat transfer efficiency and performance, and the increase in pressure drop, leading to potentially severe maintenance costs from component and system failures (Shah et al., 2009; Wright et al., 2009). To alleviate these costs, identification of ECS fouling has been the subject of many studies (Litt et al., 2004; Shang & Liu, 2010).

Focusing on ECS heat exchanger fouling identification, typical practice within the aerospace industry is to implement a system health check, known as a built-in test (BIT). Prior to flight, manually initiated built-in tests (iBIT) can be run to control the ECS with a much wider operating region (Al-Asaad & Shringi, 2000). The noteworthy time scale difference between iBITs (several minutes) and fouling (hundreds of hours) allows fouling related properties, like thermal fouling resistance and deposit thickness, to be handled as parameters, warranting the use of parameter estimation for fouling identification. Here, we propose a method that optimizes a set of system inputs to minimize the uncertainty in iBIT fouling identification, based on the Optimal Experimental Design (OED) techniques reported by Federov (2010).

The objective of the model-based approach of OED is to decrease the uncertainty of estimated model parameters while taking into account the system measurements and their variances (Bruwer & MacGregor, 2006). OED is well-established in the field of statistical design of experiments, commonly applied to enhance parameter estimation. Model-based OED uses an explicit mathematical model, which reflects our general understanding of a process with given parametric uncertainty, and can be cast as an optimization problem that maximizes future experiment information to minimize uncertainty in model parameters and system conditions. Developing an optimal iBIT can thus be formulated as an OED problem.

There exist ample applications of model-based OED. They can be applied across all engineering disciplines to any system (linear, non-linear, steady-state or dynamic). The only requirement of the model-based approach is that there must exist a model to describe the physical phenomena of the process through first principles/fundamental equations and empirical correlations, given uncertainties that are known or generally understood. This work uses a comprehensive plate fin heat exchanger model where the empirical correlations and model equations are assumed accurate and the model input uncertainty is taken into consideration. Using dynamic heat transfer analysis, the proposed method applies this OED framework to develop an optimal iBIT for fouling identification, while considering the typical operating constraints and uncertainty of an ECS.

The iBIT OED explores the sensitivities of measured heat exchanger outputs with respect to fouling-related parameters such as thermal fouling resistance and humidity. ECS inputs are then optimized to maximize these sensitivities, using a D-optimal objective function that minimizes the determinant of the variance covariance matrix of the estimated parameters (Pukelsheim, 1993; Kitsos & Kolovos, 2013). As a result, fouling can be more precisely estimated from heat exchanger measurements under noise and input uncertainty, illustrated in the following series of case studies.

METHOD OF ANALYSIS

Heat Exchanger Model Setup

The heat exchanger model was formulated with governing equations for mass, momentum, and energy balances. Gradients were assumed to be present solely along the direction of fluid flow, as flow length is notably greater than fin spacing. Fluid flow for each stream was treated as one-dimensional, while the separating crossflow plates were considered to be two-dimensional. The fluids were assumed to be ideal gases, with thermal properties unaffected by low foulant concentrations. A grid adaptation was developed for the plate fin heat exchanger that divides the system into an array of consecutive cells, shown in Figure 1. The governing equations were consequently simplified to discrete profiles through finite difference approximation. The validation and setup for this model are reported in further detail by Palmer et al. (2015).

Particulate Fouling

Fouling profiles were developed based on data reported by Abd-Elhady et al. (2011), and then applied to the plate-fin heat exchanger for fouling identification. Abd-Elhady et al. examined a diesel exhaust gas recirculation cooler (a shell-and-tube heat exchanger) to find asymptotic fouling behavior for particulate fouling as it deposits on the walls of the cooler. The shell-and-tube data was used for comparison due to lack of available information of thermal fouling resistance, R_f, patterns for plate-fin heat exchangers. A Kern and Seaton model (1959) was used to obtain an asymptotic R_f value of 6.2 × 10^{-3} m^2K/W in the experimental timeframe of the reported data, as shown in

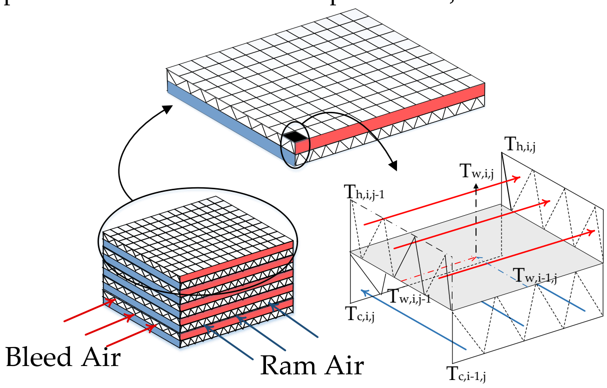

Fig. 1 Cell-by-cell discretization for the cross-flow plate-fin heat exchanger.

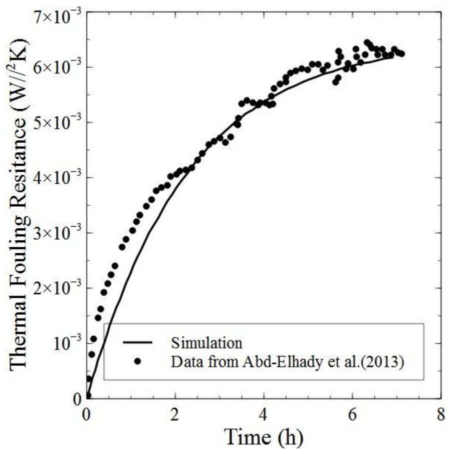

Fig. 2 Thermal fouling resistance over time reported by Abd-Elhady et al. (2011) and simulated data matched with the Kern and Seaton model (1959).

Figure 2, with estimated empirical parameters applied to the plate-fin model from Palmer et al (2015). The thermal fouling resistance observed at equilibrium was chosen as the hypothetical value to be identified through iBIT. Thermal fouling resistance for this model was calculated as the difference between the inverse of the clean and fouled convective heat transfer coefficients, shown in Eq. (1).

$$R_f = \frac{1}{U_{fouled}} - \frac{1}{U_{clean}} \quad (1)$$

Model Validation

The accuracy of the heat exchanger model was confirmed with reported cross-flow plate-fin heat exchanger data from Shah et al. (2009). The mass and energy balances of the model were compared with a small-scale apparatus (with geometry recorded in Table 1) through steady-state and dynamic heat transfer experiments. These experiments had varying flow rates and temperatures for the bleed and ram side air, with steady-state and transient heat transfer data recorded using a thermocouple placed downstream the bleed air channel.

Table 1. Core geometry and operating conditions of the heat exchanger apparatus used by Shah (2009) for tests A-H

Bleed flow length (cm)	15.24	Inlet Bleed Pressure (kPa)	240
Ram flow length (cm)	7.67	Inlet Ram Pressure (kPa)	100
Bleed fin height (mm)	6.15	Geometry Fin Type	Plain
Ram fin height (mm)	2.64	Number of cells (for both axes)	5
Plate thickness (mm)	0.599	Number of channels	4
Fin thickness (mm)	0.102	Heat Exchanger Material	Al

Table 2. Bleed outlet temperatures from experimental data reported by Shah (2009) and simulations for steady-state heat transfer.

Test	A	B	C	D
Inlet Bleed Temperature (°C)	72.8	66.7	78.2	74.6
Inlet Ram Temperature (°C)	20	20	20	20
Inlet Bleed Mass Flow (g/s)	5.22	4.85	20.41	18.33
Inlet Ram Mass Flow (g/s)	4.99	23.13	4.31	23.36
Outlet Bleed Temperature, experiment (°C)	37.4	23.4	62.9	34.8
Outlet Bleed Temperature, model (°C)	38.0	23.9	64.6	37.4

Four steady-state tests were conducted by Shah (2009) with changing bleed and ram flow rates, tests A-D shown in Table 2. The bleed outlet temperature was recorded for each test at steady-state. Transient tests were also performed as shown in case studies E-H found in Table 3. Each transient test had the heat exchanger operate at steady-state with the inlet conditions specified in Table 3. A step change of $+22°C$ was implemented to the bleed air upstream the heat exchanger, and the effects on the outlet bleed temperature were noted.

The experimental tests from Tables 2 and 3 were used to validate the steady-state and transient behavior for the heat exchanger model designed for fouling estimation. The results from the simulated steady-state tests are found in Table 2. The bleed outlet temperature data is in close alignment with the reported experimental values within $\pm 2.6°C$. Transient tests were also conducted with the heat exchanger model using reported inputs from Table 3, comparing the initial steady-state outputs and the transient responses to the step changes applied to the inlet bleed temperature. Figure 3 shows the dynamic responses of the model and the corresponding measurements reported by Shah et al. (2009). Overall, the bleed outputs match well between simulations and experiments. The bleed mass flow rates are smaller for tests E and F, causing a slower response to the step change from the inlet bleed temperature. The largest change in outlet bleed temperature was seen in test G, as it contained the highest bleed-to-ram mass flow rate ratio. For all transient tests, the responses from the simulation were slightly faster than from the experiments, most likely due to environmental heat loss as well as sensor delays that were not considered in the model (Shah, 2009). It was concluded that the model is adequate

Table 3. Initial inlet flow conditions for transient heat transfer tests E-H, reported by Shah (2009).

Test	E	F	G	H
Inlet Bleed Temperature (°C)	49.3	47	49.8	51.4
Inlet Ram Temperature (°C)	20	20	20	20
Inlet Bleed Mass Flow (g/s)	4.99	4.72	20.82	18.55
Inlet Ram Mass Flow (g/s)	4.49	23.81	4.40	22.63

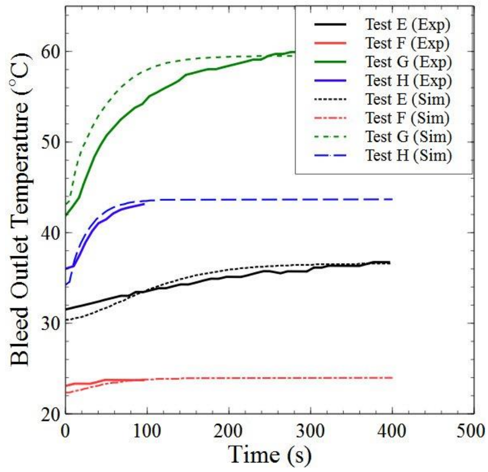

Fig. 3 Bleed outlet temperatures predicted from simulations for transient tests E-H of Table 3 with the corresponding literature data (Shah, 2009).

representing the dynamic thermal behavior of plate-fin heat exchangers.

Method Formulation

Heat exchanger fouling leads to a decrease in the overall heat transfer coefficient as well as the cross-sectional flow area, thus altering the measured exit temperatures and pressures. These measured outputs can also be affected by inputs or states such as mass flow rates, inlet pressures, inlet temperatures, etc. If any of these conditions have uncertainty and/or noise, then it is possible that these effects could in some cases be misinterpreted as fouling.

A series of uncertainties that could affect heat exchanger performance are explored in the following iBIT design case studies. To be specific, w_{H_2O} increases the fluid heat capacity for gas heat exchangers, changing outlet temperatures. $p_{hi}, \dot{m}_{hi}$ and $p_{ci}, \dot{m}_{ci}$ control the flow patterns for each fluid, which in turn impact heat transfer and pressure drop. T_{ci} has a significant effect on the exit temperatures. Without a sensor available for detecting T_{ci}, fouling estimation becomes considerably more difficult, depending on aircraft location and environmental factors. These conditions are grouped together with the thermal fouling resistance and treated as uncertain values that are estimated through case studies (see Results and Discussion) to demonstrate the capabilities of the fouling identification method proposed in this document. Uncertainty is treated as a variance interval for each uncertainty variable. These variables are given lower and upper bounds according to their feasible range. Thus, the thermal fouling resistance and uncertain inlet conditions were compiled into a vector of estimated system parameters and inputs.

$$\hat{\xi} = \hat{\boldsymbol{\theta}} \cup \hat{\mathbf{u}} = \left[R_f, w_{H_2O}, \dot{m}_{hi}, \dot{m}_{ci}, p_{hi}, p_{ci}, T_{ci} \right]. \quad (2)$$

The iBIT for the ECS was simplified by adjusting the inlet bleed temperature directly as a control input for optimal fouling detection, within the safety and design constraints of the system upstream. The inlet temperature is considered to be a series of discrete steps over time. The number of discrete step changes, n_s, and their duration, $\mathbf{t}_s$, were also adjusted to find an optimal input trajectory for estimating fouling, weighing in the complexity and timespan of the design. The duration of each step was constrained to a minimum of twenty seconds to allow steady-state to be acheived when applicable. The initial conditions, $\mathbf{y}^0$, were optimized as well, by adjusting the system states to achieve steady-state before iBIT commences. The duration of the iBIT analysis is kept relatively small to make sure that the iBIT is completed within aircraft ground handling time constraints (SAE Aerospace, 2011). The duration of the test, τ, was set to five minutes to satisfy those constraints. The inlet temperature, number and duration of step changes, and overall timespan are compiled into the test design vector, $\boldsymbol{\varphi}$.

$$\boldsymbol{\varphi} = \left[T_{hi}(t), \mathbf{t}_s, n_s, \mathbf{y}^0, \tau \right] \in \Phi . \tag{3}$$

An allowable design space Φ was assigned to the iBIT that contains upper and lower bounds for each controllable factor in Eq. (3). The heat exchanger model is expressed as a series of differential algebraic equations that are constrained to the design space of the ECS:

$$\mathbf{f}\left(\dot{\mathbf{x}}(t), \mathbf{x}(t), \mathbf{u}(t), \hat{\boldsymbol{\theta}}, t\right) = 0 . \tag{4}$$

where $\mathbf{f}$ is the system governing equations, $\mathbf{x}(t)$ is the system states (temperature and pressure), $\mathbf{u}(t)$ is the system inputs (inlet bleed temperature), and t is time. The available sensor position and type depend on ECS design, but in this case sensors are considered to be in the bleed and ram flow channels, detecting the temperature of the flows leaving the heat exchanger. The measured data is expressed as $\hat{\mathbf{y}}(t)$, which is

$$\hat{\mathbf{y}}(t) = \mathbf{h}\left(\mathbf{x}(t), \mathbf{u}(t), \hat{\boldsymbol{\theta}}\right). \tag{5}$$

The objective for optimizing the ECS iBIT is to provide the maximum available information for thermal fouling resistance, given the other uncertainties. This information comes from the sensitivities of the measured responses with respect to the estimated values $\hat{\xi}$ for all sampling times within τ. When a simulated test is completed, the sensitivities for all sampling points are placed in sensitivity matrices $\mathbf{Q}_{r,s}$, for each output, $y_{r,s}$. The experimental variance is used to factor the amount of information each output provides through the variance covariance matrix:

$$\mathbf{V}_\xi\left(\hat{\xi}, \boldsymbol{\varphi}\right) = \mathbf{H}_\xi^{-1}\left(\hat{\xi}, \boldsymbol{\varphi}\right) = \left[\sum_{r}^{n_{resp}} \sum_{s}^{n_{resp}} \tilde{\boldsymbol{\sigma}}_{rs} \mathbf{Q}_r^{T} \mathbf{Q}_s \right]^{-1}, \tag{6}$$

where $\tilde{\sigma}_{rs}$ is the rs-th element of the experimental variance matrix, and n_{resp} is the total number of measured outputs. A design criterion was set to determine how the iBIT should be optimized. For this analysis, D-opitmal design was selected to minimize the estimated uncertainty correlations from the extracted information. Doing so maximizes the capacity to isolate fouling from all other uncertain parameters and inputs:

$$\Phi_D = \arg \min_{\boldsymbol{\varphi} \in \Phi} \det\left(\mathbf{V}_\xi\left(\hat{\xi}, \boldsymbol{\varphi}\right)\right) \tag{7}$$

subject to:

$$\mathbf{f}\left(\dot{\mathbf{x}}(t), \mathbf{x}(t), \mathbf{u}(t), \hat{\boldsymbol{\theta}}, t\right) = 0,$$

$$\hat{\mathbf{y}}(t) = \mathbf{h}\left(\mathbf{x}(t), \mathbf{u}(t), \hat{\boldsymbol{\theta}}\right),$$

$$\mathbf{y}^0 = \begin{cases} \mathbf{f}\left(\dot{\mathbf{x}}(t_0), \mathbf{x}(t_0), \mathbf{u}(t_0), \hat{\boldsymbol{\theta}}, t_0\right) = 0, \\ \hat{\mathbf{y}}(t_0) = \mathbf{h}\left(\mathbf{x}(t_0), \mathbf{u}(t_0), \hat{\boldsymbol{\theta}}\right), \end{cases}$$

$$\mathbf{u}^L \le \mathbf{u}(t) \le \mathbf{u}^U$$

$$\mathbf{x}^L \le \mathbf{x}(t) \le \mathbf{x}^U \quad \forall t \in [0, \tau]$$

The optimal iBIT design vector, Φ_D, from Eq. (7) corresponds to the best test conditions for fouling identification and isolation. These results are compared to fouling estimation at nominal ECS conditions to quantify improvement from optimizing iBIT.

Tool Chain

The differential equations for the plate fin heat exchanger were set up using the object-oriented language Modelica (Modelica Association, 2010) through the commerical modeling environment Dymola (Cellier, 2015). The model was transferred from Dymola using the Functional Mockup Interface (Modelisar, 2010), a tool-independent standard. The model was compiled into a function mockup unit and then transferred into MALTAB (The Mathworks Inc., 2013) using the Modelon FMI-Toolbox (Modelon, 2014). The parametric sensitivities were calculated using the solver CVODES (Serban & Hindmarsh, 2003), a C-coded OED solver designed for sensitivity analysis through finite differences or direct approach. The optimal design was solved using NOMAD, a Mesh Adaptive Direct Search algorithm (Le Digabel, 2011).

RESULTS AND DISCUSSION

In this Section, the models and methodologies above are applied to a heat exchanger design presented by Shah and Sekuli (2003). The model of this particular heat exchanger was validated, showing good agreement, but is not presented here because the conditions in Shah and Sekuli (2003) are outside of the normal ECS range. We focus here on the methodology effectiveness rather than the correctness of the absolute values of the estimated conditions. The following case studies aim to represent the effectiveness of the proposed iBIT method under heavy fouling conditions, using the heat exchanger and fouling model described in the Method Section. This is done by simulating the heat exchanger and fouling models until the heat exchanger thermal fouling resistance reaches a value of 6.2×10^{-3} m^2K/W, based on Figure 2. It is assumed that fouling is significant at this time and must be identified. For identification, an iBIT is ran at nominal (typical operation inputs) and optimal (OED determined inputs) conditions, and the capability to identify fouling with certainty is explored for each iBIT, respectively. A "virtual system" and a "system model" are used for fouling identification, describing the state of significant fouling with noisy responses and the predicted behavior without noise, respectively.

Basis for Heat Exchanger Fouling Analysis

The ECS heat exchanger system was set to nominal conditions for each case study. These conditions are specified in Table 4, and are considered typical for an primary aircraft air-cooled heat exchanger. The inlet bleed temperature was adjusted according to the iBIT design, constrained between 100°C and 250°C. It was assumed that adjusting the inlet bleed temperature caused no issues on ECS performance upstream. The ram inlet temperature varies based on location, day type and altitude of the aircraft. For these tests, the ram inlet temperature was assumed to be the international standard atmospheric value at sea level, according to the International Standard Aviation Organization (International Civil Aviation Organization, 1993).

Table 4. ECS conditions for the fouling estimation case studies.

Flow Condition	Nominal Setting
T_{hi} (°C)	175
T_{ci} (°C)	15
$\dot{m}_{hi}$ (kg/s)	0.30
$\dot{m}_{ci}$ (kg/s)	1.00
p_{hi} (kPa)	250
p_{ci} (kPa)	100

The thermal fouling resistance and uncertain flow conditions were predicted in several case studies. 95% confidence intervals were obtained and compared for nominal and optimal conditions to evaluate the robustness of the proposed iBIT fouling identification method. $\tilde{\sigma}$ was assigned zero-mean white measurement noise with a standard deviation of 0.5°C for each temperature. Noise-free simulations were set up in the system model, and were adjusted with $\hat{\xi}$ to match the experimental data from the virtual system. Fouling estimation was conducted with least-squares estimation (LSE), minimizing the sum of squared residuals between simulated and experimental outputs by adjusting predicted fault-related variables. Only temperature measurements were compared for these studies, as it is more common to have temperature sensors available in an ECS. It was assumed that the temperature sensors placed downstream were well-calibrated and adequately positioned to detect deviations in heat transfer. Pressure sensors and mass flow sensors do not exist the ECS channels directly before or after heat exchangers, so pressure and mass flow information was not used for these case studies. Each estimated inlet condition was constrained to ±25% of their nominal value after uncertainty.

Identification of Fouling in an Uncertainty-Free System

We first explored the robustness of the proposed iBIT method for an ideal uncertainty-free system to identify the parametric fault of heat exchanger fouling. The optimal iBIT design yielded an inlet temperature at the upper bound of its allowable range (250 °C). For this iBIT, only one temperature step was used throughout its duration, τ. Any additional input steps did not significantly improve the estimation accuracy of thermal fouling resistance.

The effect of system inlet conditions on fouling identification is illustrated in Figure 4, showing the difference between clean and fouled heat exchanger operation at nominal and optimal conditions. The solid green line in Figure 4 is the inlet bleed temperature, shown to illustrate the distance between nominal and optimal iBIT conditions estimated by Eq. (7). Figure 4 was generated by initializing the virtual system at a nominal steady-state followed by simulation for 300s. The inlet bleed temperature was then changed to the value estimated by Eq. (7) (250 °C) and the virtual system was simulated for another 600s. The virtual system transitions smoothly from the nominal iBIT steady-state to the optimal iBIT steady-state, shown in the transient response of Figure 4.

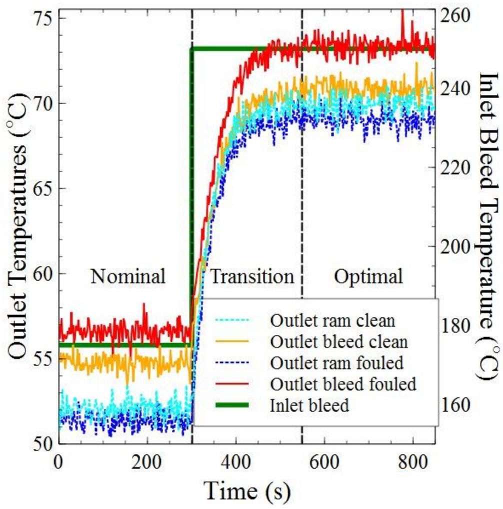

Fig. 4 Inlet bleed temperature and predicted outlet ram and bleed temperatures of a clean and fouled heat exchanger. The heat exchanger is initially set to steady-state at nominal conditions for 300s and then transitioned to the steady-state of the optimal iBIT settings. The optimal test is simulated for 300s.

The inlet bleed temperature is higher for the optimal iBIT, resulting in an increased rate of heat transfer. Thermal fouling resistance has a more observable effect on heat exchanger effectiveness at higher heat transfer rates, enhancing the identifiability of fouling. It is clear from Figure 4 that there is an increase in the absolute temperature difference of the outlet bleed stream between the clean and fouled heat exchanger responses, also between the nominal and optimal iBIT. The heat transfer effectiveness of the fouled heat exchanger is deteriorated when compared to the clean heat exchanger case. This is more evident when the heat transfer requirement is higher which is demonstrated from the optimal iBIT.

Estimating the thermal fouling resistance of the virtual system at nominal and optimal iBIT conditions, using the iBIT data and the system model, produced R_f values of $6.26\pm0.37\times10^{-3}$ and $6.19\pm0.25\times10^{-3}$ m^2K/W, respectively. The inlet ram temperature of an aircraft depends on the location of the aircraft and the time of day; therefore, the thermal fouling resistance was also estimated for inlet ram temperatures of $-50°C$ and $40°C$ to account for the scenarios of fouling identification during cold and hot atmospheric conditions, which have varying effects on the heat transfer rate. The results showed no significant effect on the corresponding estimates of thermal fouling resistance when compared to that produced by the standard inlet ram temperature (15 °C). Regardless of the atmospheric conditions, the above shows that the estimated value of thermal fouling resistance and its confidence intervals were improved, albeit slightly, through the optimal iBIT (manipulation of inlet bleed temperature).

Table 5. MTD values for clean and fouled conditions for the nominal and optimal iBIT runs for Case Study I.

Stream Duct	Clean Nominal	Fouled Nominal	Clean Optimal	Fouled Optimal
T_{ci} (°C)	20	20	20	20
T_{co} (°C)	52	51.5	70	69
T_{hi} (°C)	175	175	250	250
T_{ho} (°C)	55	56.5	71	73.5
T_{mtd} (°C)	58.3	60.4	83.1	87.0
Q (kW)	36.2	35.7	54.0	53.2
UA (W/K)	621	591	651	611

Another way to demonstrate the effectiveness of optimizing fouling identification during iBIT is shown in Table 5, comparing the mean temperature difference (MTD) and the overall heat transfer coefficient for the same nominal and optimal cases used to generate the data shown in Figure 4. The MTD was found by calculating the log mean temperature difference between adjacent streams ducts while factoring in a correction coefficient for cross-flow heat exchanger geometry. Fouling causes less heat to be transferred between streams, thus MTD increases with fouling. The change in MTD caused by fouling is 2.1°C for the nominal case and 3.9°C for the optimal case. The percent deviation in MTD due to fouling is 3.6% and 4.7%, respectively. UA, the overall heat transfer coefficient multiplied by the effective heat transfer area, was also calculated from the model. Similar to Q, UA decreases with fouling, more so in the optimal case than in the nominal, confirming that there is an increase to fouling sensitivity at higher temperatures. The deviations from the expected MTD and UA values, caused by the same level of fouling in an uncertainty-free system, were more prominent through the optimal iBIT.

Heat Exchanger Fouling with Uncertainty in the Air Moisture Content

Moisture content is a common source of uncertainty in ECS fouling detection. In this case study, it is considered that the moisture content affects the fluid behavior of the bleed and ram streams by changing the overall heat capacity. It is also assumed that there is no condensation present in the heat transfer surfaces. The maximum atmospheric humidity at 15°C is 1.2 wt% assuming no precipitation, according to psychrometric charts by Felder & Rousseau (2004), and the minimum absolute humidity is 0.1 wt%. The weighted average found for the fluid heat capacities using dry air correlations from Smith et al. (2005), while considering 0.1 to 1.2 wt% of moisture, to produce a range of 1005 to 1043 J/kg K at 15°C, and 1048 to 1085 J/kg K at 250°C. The optimal iBIT problem was developed for this case study classifying both thermal fouling resistance and the fluid heat capacities as unknowns with the assigned ranges listed above.

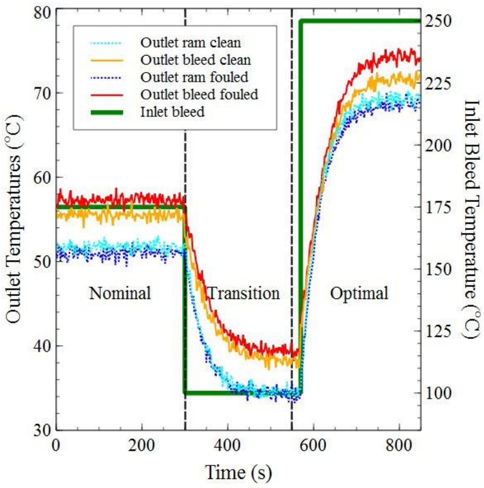

Fig. 5 Inlet bleed temperature and predicted outlet ram and bleed temperatures of a clean and fouled heat exchanger with a moisture content of 1.2 wt%. The heat exchanger is initially set to steady-state at nominal conditions for 300s and then transitioned to the steady-states of the optimal iBIT settings (100→250 °C). The optimal final test is simulated for 300s.

The virtual system temperature of the ram and bleed outlets are shown in Figure 5 for a heat exchanger system with the ambient air at maximum humidity level for nominal and optimal conditions. The presentation of the data is in a similar format to Figure 4. Fluid flows at minimum humidity levels were simulated as well, with similar effects that are not shown in this report. The iBIT was optimized by establishing two control steps (n_s=2) with two different temperatures to separate the effects of thermal fouling resistance and unknown humidity level in the system. The first control step was assigned a duration of 20s at the lower inlet temperature bound, while the second control step was set to the upper bound for 280s. With two significantly contrasting states, the model is able to predict more effectively the convective and advective aspects of heat transfer inside the heat exchanger, which in turn are dependent on the fluid specific heat capacity. A transition was set between the nominal and optimal conditions to attain optimum steady-state for the first inlet step.

The moisture content and thermal fouling resistance were estimated from the experimental data by observing the steady-state and dynamic effects during the optimal test. At nominal (steady-state) conditions, in the timeframe of t=0 to 300s in Figure 5, the thermal fouling resistance and moisture content were estimated at 5.90±12.3×10^{-3} m^{2}K/W and 1.21±5.41 wt%, respectively. Through optimal iBIT, the simulated model predicted estimates for R_f and w_{H_2O} at 6.03±0.21×10^{-3} m^{2}K/W and 1.27±0.11 wt%. The confidence regions of the estimates for the nominal design were considerably larger, to such a point that the intervals contain negative values of moisture and fouling. Fouling estimation during these conditions is considered to be practically infeasible, indicating the need to apply a structured iBIT design strategy that can improve estimation precision for fouling detection and isolation.

This case study also illustrates the effect on the objective function output at nominal and optimal conditions. To reiterate, the objective function for estimating fouling minimizes the sum of squared residuals between the virtual experimental and simulated outputs. The objective function output was computed over the entire allowable space of thermal fouling resistance and moisture content values. Figure 6 shows how the objective function changes with estimated parameter values at nominal and optimal iBIT settings. The nominal case contains a notably large valley of similar outputs surrounding the true values of R_f and w_{H_2O}, displaying numerous potential conditions that can be estimated for a given response, making fouling virtually unidentifiable. In the optimal iBIT, it can be seen that the number of similar outputs is significantly reduced, thus improving the likelihood of accurate estimation for R_f and w_{H_2O}.

Further Analysis of Heat Exchanger Fouling with Uncertainty in Various Inlet Conditions

The thermal fouling resistance was estimated with additional uncertain parameters, namely mass flows and a combination of moisture content, ram mass flow rate and ram inlet temperature. Fouling identifiability decreased when the mass flow rates were uncertain, quantified by the lack of accuracy in the estimates at nominal conditions and their wide confidence intervals. System flow rates have a significant impact on fouling identification, due to their influence on heat transfer effectiveness. Nonetheless, a vast improvement was feasible with the optimal iBIT strategy. When the inlet ram temperature, inlet ram mass flow, humidity, and thermal fouling resistance were treated as uncertain, the task of using iBIT to estimate system fouling became a large-scale multi-variable optimization problem. The results of this case study show the greatest improvement in estimating uncertain inputs and fouling levels, indicating that the iBIT benefits the most from optimizing conditions for fouling identification when there are multiple uncertainties present.

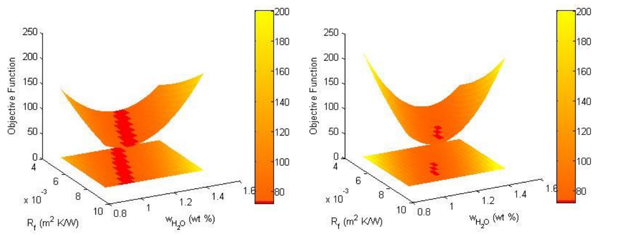

Fig. 6 Objective function values of the parameter estimation problem over a range of system model thermal fouling resistance and moisture content values using nominal (left) and optimal (right) iBIT settings. The dark squares represent the estimated parameters that correspond to the correct system output (the minimum objective function)

CONCLUSIONS

1. An iBIT method was formulated for aircraft plate fin heat exchanger fouling identification utilizing a D-optimal experimental design framework.
2. The proposed iBIT methodology allows for accurate and precise estimation of heat exchanger fouling that would have been infeasible with other conventional methods, without the addition of extra measurement devices or other iBIT equipment.
3. Future work will focus on the significance of transient analysis on iBIT, the development of structural local and global identifiability tests and the effects of bias and sensor placement.

ACKNOWLEDGEMENT

This work was sponsored by the UTC Institute for Advanced Systems Engineering (UTC-IASE) of the University of Connecticut and the United Technologies Corporation. Any opinions expressed herein are those of the authors and do not represent those of the sponsor. Help and guidance by Modelon and Modelon-AB are gratefully acknowledged.

NOTATION

A Heat transfer surface area (m^2)
$\mathbf{f}$ Governing system of equations (varies)
$\mathbf{h}$ Measured output function (varies)
$\mathbf{H}_\xi$ Fisher information matrix (dimensionless)
$\dot{m}$ Mass flow rate (kg/s)
n_s Number of step changes (dimensionless)
n_{resp} Number of output responses (dimensionless)
N_{sp} Number of sampling points (dimensionless)

p Pressure (Pa)
$\mathbf{Q}_{r,s}$ Sensitivity matrix (varies)
Q Heat transfer (kW)
R_f Thermal fouling resistance (m^2 K/ W)
T Temperature (°C)
t Time (s)
$\mathbf{t}_{sp}$ Sampling time vector (s)
$\mathbf{u}$ Input vector (°C)
U Convective heat transfer coefficient (W/m^2 K)
$\mathbf{V}_{\xi}$ Variance-covariance matrix (dimensionless)
w_{H2O} Water mass fraction (dimensionless)
$\mathbf{x}$ System state vector (varies)
$\hat{\mathbf{y}}$ Measured system outputs (°C)
$\mathbf{y}^0$ Initial conditions (varies)
φ Experimental design vector (varies)
Φ Experimental design constraints (varies)
Φ_D D-optimal output (dimensionless)
$\tilde{\sigma}$ Measurement variance (°C)
τ Experiment duration (s)
$\hat{\boldsymbol{\theta}}$ Estimated parameters vector (varies)
ξ Fault-related variables vector (varies)

Subscript
c Ram fluid side
h Bleed fluid side
i Inlet
o Outlet
mtd Mean temperature difference

REFERENCES

Abd-Elhady, M. S. S., Zornek, T., Malayeri, M. R. R., Balestrino, S., Szymkowicz, P. G. G., & Müller-Steinhagen, H. (2011). Influence of gas velocity on particulate fouling of exhaust gas recirculation coolers. *International Journal of Heat and Mass Transfer*, *54*(4), 838–846.

Al-Asaad, H., & Shringi, M. (2000). On-line built-in self-test for operational faults. *2000 IEEE Autotestcon Proceedings. IEEE Systems Readiness Technology Conference. Future Sustainment for Military Aerospace (Cat. No.00CH37057)*, 168–174.

Bruwer, M.-J., & MacGregor, J. F. (2006). Robust multi-variable identification: Optimal experimental design with constraints. *Journal of Process Control*, *16*, 581–600.

Cellier, F. E. (2015). Dymola: Environment for Object-oriented Modeling of Physical Systems. Lund, Sweden: Dassault Systemes AB.

Fedorov, V. (2010). Optimal Experimental Design. *Wiley Interdisciplinary Reviews: Computational Statistics*, *2*(5), 581–589.

Felder, R. M., & Rousseau, R. W. (2004). *Elementary Principles of Chemical Processes* (3rd Edition.). Wiley.

International Civil Aviation Organization. (1993). *Manual of the ICAO Standard Atmosphere (extended to 80 kilometres (262 500 feet))* (3rd Edition.). Montreal, Canada.

Kays, W. M., & London, A. L. (1984). *Compact Heat Exchangers* (3rd ed.). New York: McGraw-Hill.

Kern, D. Q., & Seaton, R. E. (1959). A Theoretical Analysis of Thermal Surface Fouling. *British Chemical Engineering*, *4*(5), 258–262.

Kitsos, C. P., & Kolovos, K. G. (2013). A Compilation of the D-Optimal Designs in Chemical Kinetics. *Chemical Engineering Communications*, *200*(2), 185–204.

Le Digabel, S. (2011). Algorithm 909: {NOMAD}: Nonlinear optimization with the {MADS} algorithm. *ACM Transactions On Mathematical Software*, *37*(4), 44:1–44:15.

Litt, J. S., Simon, D. L., Garg, S., Guo, T.-H., Mercer, C., Millar, R., … Jensen, D. T. (2004). A Survey of Intelligent Control and Health Management Technologies for Aircraft Propulsion Systems. *Journal of Aerospace Computing, Information, and Communication*, *1*(12), 543–563.

Modelica Association. (2010). Modelica® - A Unified Object-Oriented Language for Physical Systems Modeling. Linköping, Sweden: Modelica Association.

Modelisar. (2010). Functional Mock-up Interface for Model Exchange, Version 1.0.

Modelon. (2014). FMI Toolbox for MATLAB/Simulink, Version 1.8.2. Lund, Sweden: Modelon AB.

Moir, I., & Seabridge, A. (2008). *Aircraft Systems* (3rd ed.). West Sussex, England: John Wiley & Sons, Ltd.

Palmer, K. A., Hale, W. T., Such, K. D., Shea, B. R., & Bollas, G. M. (2015). A Structured Method for Plate-Fin Heat Exchanger Fouling Identification. *Applied Thermal Engineering*, *in review*.

Pérez-Grande, I., & Leo, T. J. (2002). Optimization of a commercial aircraft environmental control system. *Applied Thermal Engineering*, *22*(17), 1885–1904.

Pukelsheim, F. (1993). *Optimal Experimental Design*. New York: John Wiley & Sons, Inc.

SAE Aerospace. (2011). *Aerospace Information Report 1266 Rev. A - Fault isolation in environmental control systems of commercial transports*.

Serban, R., & Hindmarsh, A. C. (2003). CVODES: the Sensitivity-Enabled ODE Solver in SUNDIALS. *ACM Transactions on Mathematical Software*, *5*, 1–18.

Shah, R. K., & Sekuli, D. P. (2003). *Fundamentals of Heat Exchanger Design*. Hoboken, NJ, USA: John Wiley & Sons, Inc.

Shah, S. A. (2009). *Modeling and Fouling Detection of the Aircraft Environmental Control System Heat Exchanger*. Ryerson University.

Shah, S., Liu, G., & Greatrix, D. R. (2009). Modelling , simulation , and experimental evaluation of a crossflow heat exchanger for an aircraft environmental control system. *Aerospace Engineering*, *224*(G), 613–623.

Shang, L., & Liu, G. (2010). Heat exchanger fouling detection in a simulated aircraft engine bleed air temperature control system.

Smith, J.M., Van Ness, H.C., Abbott M.M. (2005). *Introduction to Chemical Engineering Thermodynamics* (7th ed.), New York: McGraw-Hill.

The Mathworks Inc. (2013). Matlab. Natick, MA: The MathWorks Inc.

Wright, S., Andrews, G., & Sabir, H. (2009). A review of heat exchanger fouling in the context of aircraft air-conditioning systems, and the potential for electrostatic filtering. *Applied Thermal Engineering*, *29*(13), 2596–2609.